Letter

Rapidly rotating self-gravitating Boussinesq fluid. III. A previously unknown zonal oscillation at the onset of rotating convection

Wenbo Li
State Key Laboratory of Lunar and Planetary Sciences, Macau University of Science and Technology, Taipa, Macao 999078, China

Dali Kong*
CAS Key Laboratory of Planetary Sciences, Shanghai Astronomical Observatory, Chinese Academy of Sciences, Shanghai 200030, China

(Received 1 November 2022; accepted 20 January 2023; published 30 January 2023)

Realistic rotating fluid under self-gravitation will be oblate due to the centrifugal force. In our previous paper [Li and Kong, Phys. Rev. Fluids **7**, 103502 (2022)], for the first time, the problem of convective instabilities was formulated and tackled in rotationally flattened spheroids. Using that method, this paper demonstrates how extraordinary nonsphericity alters the linear onset of thermal inertial convection in internally heated Boussinesq fluid. A significant discovery is that the globally most unstable mode could switch from a non-axisymmetric quasigeostrophic wave to an equatorially symmetric zonal oscillation when the rotational flattening effect gets very strong. This was the only form of global convection not found so far.

DOI: 10.1103/PhysRevFluids.8.L011501

I. INTRODUCTION

Chandrasekhar [1] first formulated the problem of thermal instabilities in self-gravitating, internally heated, rapidly rotating Boussinesq fluid spheres and spherical shells under the assumption that the convective mode at the onset of thermal instability is axisymmetric, which was later demonstrated to not be the most unstable mode in the regime of asymptotically small Ekman numbers. Roberts [2] first extended the consideration of the problem to the general non-axisymmetric case. But as pointed out by Busse [3], Roberts's non-axisymmetric mode would not be physically preferred at the onset of rotating convection because of the selected equatorial antisymmetry. Busse corrected the view and determined the globally most unstable mode at the onset of convection should be non-axisymmetric and equatorially symmetric in a rapidly rotating Boussinesq fluid sphere. This understanding remained until Garcia *et al.* [4] discovered non-axisymmetric and equatorially antisymmetric polar modes in rotating spherical fluid shells. More recently, Sánchez Umbría *et al.* [5] found that an axisymmetric and equatorially antisymmetric torsional oscillation mode could be the globally most unstable in an internally heated rotating fluid sphere, subject to the stress-free velocity boundary condition.

All the abovementioned researchers and many others have adopted spherical approximation in their modeling, but many gaseous giant planets and luminous stars rotate extremely fast and hence are significantly flattened [6,7].

Based on an oblate spheroidal model of conduction state developed by Kong [8], the problem of thermal instability in rotating oblate spheroidal fluid cavities was formulated and tackled by Li and

*dkong@shao.ac.cn

Kong [9]. It is now time to investigate how the departure of a rapidly rotating, self-gravitating fluid domain from sphericity may alter the symmetry of the onset of rotating convection. In this Letter, we briefly report an outstanding example in which the physically preferred mode at the linear onset of thermal convection surprisingly becomes an equatorially symmetric zonal oscillation, when the nonsphericity exceeds a certain level. This is the last form of previously unknown global convection.

Because detailed derivations have already been shown in our previous two papers, Kong [8] and Li and Kong [9], only the critical ideas of analyzing the nonspherical problem of thermal instabilities are discussed in Sec. II. Analytical results and the corresponding numerical results are presented in Sec. III. Section IV concludes this Letter.

II. THERMAL INSTABILITY IN SIGNIFICANTLY FLATTENED OBLATE SPHEROIDS

Consider a Boussinesq fluid with the constant thermal expansion coefficient α, constant thermal diffusivity κ, and constant kinematic viscosity ν. The fluid is confined within an oblate spheroidal cavity rotating about the symmetry axis at a constant angular velocity of $\mathbf{\Omega} = \Omega\hat{\boldsymbol{z}}$. The eccentricity $\mathcal{E} = \sqrt{R_e^2 - R_p^2}/R_e$ is calculated from the equatorial radius R_e and the polar radius R_p and hence represents the oblateness. The Froude number $\mathrm{Fr} = 3\Omega^2/(4\pi \mathrm{G}\rho_0)$ measures the importance of the centrifugal force relative to the self-gravitation of the fluid. According to the classical Maclaurin spheroid relation [10], the geometrical shape is determined by the Froude number such that the fluid and the cavity can be in a rotational equilibrium state. Uniformly distributed heat sources internally heat the fluid. When the heating is not sufficiently strong, the state ought to be stably stratified and can be described by

$$\rho_0 \mathbf{\Omega} \times (\mathbf{\Omega} \times \boldsymbol{r}) = -\nabla P_0(\boldsymbol{r}) + \rho_0 \boldsymbol{g}_0(\boldsymbol{r}), \tag{1}$$

$$\nabla \cdot \boldsymbol{g}_0(\boldsymbol{r}) = -4\pi G\rho_0, \tag{2}$$

$$\nabla^2 T_0 + \beta = 0, \tag{3}$$

in which $\boldsymbol{g}_0$, T_0, and P_0 are the equilibrium gravity, temperature, and pressure, respectively, and the constant β represents the heat sources. By virtue of oblate spheroidal coordinates ($0 \leqslant \eta \leqslant \sqrt{1-\mathcal{E}^2}$, $0 \leqslant \phi < 2\pi$, $-1 \leqslant \tau \leqslant 1$) with unit vectors ($\hat{\boldsymbol{\eta}}$, $\hat{\boldsymbol{\phi}}$, $\hat{\boldsymbol{\tau}}$), which admit the transformation below to the familiar Cartesian coordinates

$$\begin{aligned} x &= R_e\sqrt{(\eta^2+\mathcal{E}^2)(1-\tau^2)}\cos\phi, \\ y &= R_e\sqrt{(\eta^2+\mathcal{E}^2)(1-\tau^2)}\sin\phi, \\ z &= R_e\eta\tau, \end{aligned}$$

as elucidated in Kong [8], the conduction state can be solved from Eqs. (1)–(3), subject to an equipotential boundary condition for gravitational plus centrifugal potential and the zero boundary conditions for both the temperature and the pressure,

$$\frac{2\mathrm{Fr}}{3} = \frac{\sqrt{1-\mathcal{E}^2}}{\mathcal{E}^3}(3-2\mathcal{E}^2)\sin^{-1}\mathcal{E} - \frac{3(1-\mathcal{E}^2)}{\mathcal{E}^2}, \tag{4}$$

$$\hat{\boldsymbol{\eta}} \cdot \boldsymbol{g}_0 = \gamma R_e \frac{3\eta}{2\mathcal{E}^3}\frac{\sqrt{\eta^2+\mathcal{E}^2}}{\sqrt{\eta^2+\mathcal{E}^2\tau^2}}[\mathcal{E} - 3\mathcal{E}\tau^2 - \mathcal{E}^3(1-\tau^2) + \sqrt{1-\mathcal{E}^2}(3\tau^2-1)\sin^{-1}\mathcal{E}], \tag{5}$$

$$\hat{\boldsymbol{\tau}} \cdot \boldsymbol{g}_0 = \gamma R_e \frac{3\tau}{2\mathcal{E}^3}\frac{\sqrt{1-\tau^2}}{\sqrt{\eta^2+\mathcal{E}^2\tau^2}}[\mathcal{E}^5 - \mathcal{E}^3 + \mathcal{E}(\mathcal{E}^2-3)\eta^2 + \sqrt{1-\mathcal{E}^2}(3\eta^2+\mathcal{E}^2)\sin^{-1}\mathcal{E}], \tag{6}$$

$$T_0 = \beta R_e^2 \frac{[1-(\eta^2+\mathcal{E}^2)][1-\mathcal{E}^2(1-\tau^2)]}{6-4\mathcal{E}^2}, \tag{7}$$

in which $\gamma = 4\pi G\rho_0/3$.

When the heat sources get sufficiently strong, thermal instability drives convective motion that slightly modifies the conduction state. The linearized dimensionless equations governing the weak convection problem near onset are

$$\frac{\partial \boldsymbol{u}}{\partial t} + 2\hat{\boldsymbol{z}} \times \boldsymbol{u} = -\nabla p + \mathrm{St}(2\mathrm{Fr} - 3)\Theta \nabla \mathrm{T}_0 + \mathrm{Ek}\nabla^2 \boldsymbol{u}, \tag{8}$$

$$\nabla \cdot \boldsymbol{u} = 0, \tag{9}$$

$$\frac{\partial \Theta}{\partial t} + \boldsymbol{u} \cdot \nabla T_0 = \frac{\mathrm{Ek}}{\mathrm{Pr}} \nabla^2 \Theta, \tag{10}$$

where Θ represents the temperature fluctuation, p is the reduced pressure, and $\boldsymbol{u}$ is the velocity of convection. We have employed R_e as the length scale, Ω^{-1} as the timescale, and βR_e^2 as the temperature unit. The three key nondimensional parameters, the stratification number St, the Prandtl number Pr, and the Ekman number Ek, are defined as

$$\mathrm{St} = \frac{\alpha\beta\gamma \mathrm{R_e^2}}{\Omega^2}, \quad \mathrm{Pr} = \frac{\nu}{\kappa}, \quad \mathrm{Ek} = \frac{\nu}{\Omega \mathrm{R_e^2}}.$$

The equations are equipped with the no-slip and isothermal boundary conditions for velocity and temperature fluctuation on the bounding surface $\mathcal{S} = \{(\eta, \phi, \tau) | \eta = \sqrt{1 - \mathcal{E}^2}\}$.

In the regime of asymptotically small Ekman numbers $0 < \mathrm{Ek} \ll 1$ and sufficiently small Prandtl numbers, a global asymptotic analysis was carried out in Li and Kong [9], showing that the convective motion at onset is marked by one dominant inertial mode in the oblate spheroidal cavity. As explained therein, the primary interior flow is nondissipative, while the buoyancy force drives thermal convection against viscous dissipation in the boundary layer.

The asymptotic solution can be expanded by

$$\boldsymbol{u} = \mathcal{A}\{[\widehat{\boldsymbol{u}} + \boldsymbol{u}_{mnk}(\eta, \phi, \tau)] + \widetilde{\boldsymbol{u}}\} e^{i2\sigma t} + \mathrm{c.c.} + \cdots, \tag{11}$$

$$p = \mathcal{A}\{[\widehat{p} + p_{mnk}(\eta, \phi, \tau)] + \widetilde{p}\} e^{i2\sigma t} + \mathrm{c.c.} + \cdots, \tag{12}$$

$$\Theta = \mathcal{A}\Theta_0(\eta, \phi, \tau) e^{i2\sigma t} + \mathrm{c.c.} + \cdots, \tag{13}$$

$$\mathrm{St} = \mathrm{St}_1 + \cdots, \tag{14}$$

$$\sigma = \sigma_{mnk} + \sigma_1 + \cdots, \tag{15}$$

where $i = \sqrt{-1}$; σ denotes the half frequency; $\mathcal{A}$ represents the amplitude of convection; $\boldsymbol{u}_{mnk}$, p_{mnk}, and σ_{mnk} are the flow, pressure, and half eigenfrequency of the primary inertial mode (see Zhang *et al.* [11] for the explicit formulas), respectively; the boundary flow $\widetilde{\boldsymbol{u}}$ and the associated pressure $\widetilde{p}$ only exist in the thin boundary layer where $|\widetilde{\boldsymbol{u}}| = O(|\boldsymbol{u}_{mnk}|)$; and $\widehat{\boldsymbol{u}}$ and $\widehat{p}$ are the small secondary interior perturbations caused by the boundary flow and vanish in the boundary layer. σ_1 is the small correction to the half eigenfrequency of the inertial mode, which is determined with St_1 in the following analysis. c.c. denotes the complex conjugate of the previous term. The order m denotes the azimuthal wave number. At the same time, n and k roughly outline the complexity of the flow structure in the directions perpendicular to and parallel to the rotation axis. The temperature Θ_0, driven by a spheroidal inertial mode $\boldsymbol{u}_{mnk}$, can be expanded by the radial spheroidal wave functions of the first kind $R_{ml}^{(1)}(-i\mathcal{E}k_{lq}, i\eta/\mathcal{E})$ and the spheroidal angular functions $S_{ml}^{(1)}(-i\mathcal{E}k_{lq}, \tau)$ of the first kind, which are the eigenfunctions of the Helmholtz equation $\nabla^2\psi + k^2\psi = 0$ in an oblate

spheroidal domain [12], in the form

$$\Theta_0 = -\sum_{l,q} \frac{R_{ml}^{(1)}(-i\mathcal{E}k_{lq}, i\eta/\mathcal{E}) S_{ml}^{(1)}(-i\mathcal{E}k_{lq}, \tau)}{k_{lq}^2 \mathrm{Ek/Pr} + \mathrm{i}2\sigma_{\mathrm{mnk}}}$$

$$\times\ 2\pi \int_{-1}^{1} \int_{0}^{\sqrt{1-\mathcal{E}^2}} (\boldsymbol{u}_{\mathrm{mnk}} \cdot \nabla \mathrm{T}_0) \mathrm{R}_{\mathrm{ml}}^{(1)}(-\mathrm{i}\mathcal{E}\mathrm{k}_{\mathrm{lq}}, \mathrm{i}\eta/\mathcal{E}) \mathrm{S}_{\mathrm{ml}}^{(1)}(-\mathrm{i}\mathcal{E}\mathrm{k}_{\mathrm{lq}}, \tau)(\eta^2 + \mathcal{E}^2\tau^2) \mathrm{d}\eta \mathrm{d}\tau, \quad (16)$$

where k_{lq} are determined by zeros of $R_{ml}^{(1)}$ functions,

$$R_{ml}^{(1)}(-i\mathcal{E}k_{lq}, i\sqrt{1-\mathcal{E}^2}/\mathcal{E}) = 0, \quad (17)$$

with k_{lq} being ordered such that $0 < k_{l1} < k_{l2} < k_{l3} < \cdots$. The spheroidal wave functions $R_{ml}^{(1)}(-i\mathcal{E}k_{lq}, i\eta/\mathcal{E})$ and $S_{ml}^{(1)}(-i\mathcal{E}k_{lq}, \tau)$ have been normalized as

$$\int_0^{2\pi} \int_{-1}^{1} \int_{0}^{\sqrt{1-\mathcal{E}^2}} R_{ml}^{(1)}(-i\mathcal{E}k_{lq}, i\eta/\mathcal{E}) S_{ml}^{(1)}(-i\mathcal{E}k_{lq}, \tau)$$

$$\times R_{ml'}^{(1)}(-i\mathcal{E}k_{l'q'}, i\eta/\mathcal{E}) S_{ml'}^{(1)}(-i\mathcal{E}k_{l'q'}, \tau)(\eta^2 + \mathcal{E}^2\tau^2) d\eta d\tau \mathrm{d}\phi = \delta_{ll'}\delta_{qq'}.$$

For any given Ekman number Ek that is asymptotically small, Prandtl number Pr that is sufficiently small, and Froude number Fr that obeys the Maclaurin spheroid relation, the physically preferred mode at the onset of convection (p_{mnk}, $\boldsymbol{u}_{mnk}$, Θ_0) associated with the unknown values of (m, n, k) is determined through the solvability condition of the next-order problem described by

$$i2\sigma_{mnk}\widehat{\boldsymbol{u}} + 2\hat{\boldsymbol{z}} \times \widehat{\boldsymbol{u}} + \nabla \widehat{p} = \mathrm{St}_1(2\mathrm{Fr} - 3)\Theta_0 \nabla \mathrm{T}_0 + \mathrm{Ek}\nabla^2 \boldsymbol{u}_{\mathrm{mnk}} - \mathrm{i}2\sigma_1 \boldsymbol{u}_{\mathrm{mnk}}, \quad (18)$$

$$\nabla \cdot \widehat{\boldsymbol{u}} = 0, \quad (19)$$

and the secondary flow $\widehat{\boldsymbol{u}}$ is subject to the boundary condition

$$\hat{\boldsymbol{\eta}} \cdot \widehat{\boldsymbol{u}} = \mathrm{influxattheouteredgeoftheviscousboundarylayer}\widetilde{\boldsymbol{u}}. \quad (20)$$

The explicit expression of the boundary flow $\widetilde{\boldsymbol{u}}$, which can be obtained from solving standard boundary layer equations (see the Appendix of Li and Kong [9]), enters Eqs. (18) and (19) through Eq. (20). In this order, thermal effects are coupled with the nondissipative thermal-inertial mode, driving convection against viscous dissipation. Since Eq. (18), whose right-hand side is related to the leading-order solution ($\boldsymbol{u}_{mnk}$, Θ_0), is inhomogeneous, it requires a solvability condition whose real part yields an expression for the stratification number St_1. In contrast, the imaginary part can be used to determine σ_1.

The globally minimum critical stratification number $\mathrm{St_c}$ is determined by minimizing St_1 over different inertial modes $\boldsymbol{u}_{mnk}$, giving rise to the most unstable mode $\boldsymbol{u}_{m_c n_c k_c}$ marked by the critical wave numbers $m = m_c$, $n = n_c$, and $k = k_c$ along with the corresponding half eigenfrequency $\sigma_c = \sigma_{m_c n_c k_c} + \sigma_1$.

III. RESULTS AND NUMERICAL VERIFICATIONS

We try the parameters $\mathrm{Ek} = 10^{-4}$ and $\mathrm{Pr} = 5 \times 10^{-3}$. The asymptotic solutions developed in this paper are computed for several inertial modes in highly flattened spheroids. The eccentricity ranges between $0.8 \leqslant \mathcal{E} \leqslant 0.9$. As shown in Fig. 1, the critical stratification numbers of the modes are plotted against the oblateness $\mathcal{E}$. A remarkable crossover is predicted at about $\mathcal{E} = 0.84$. Below this oblateness, the globally most unstable mode at the onset of rotating convection should still be the (2,1,1) quasigeostrophic wave mode, which is consistent with the classical understanding that the preferred mode at the onset of rotating convection in a globe is non-axisymmetric and equatorially symmetric. But above this oblateness, surprisingly, the axisymmetric and equatorially symmetric (0,1,2) oscillatory mode seems to become the physically preferred one. The explicit form of the leading-order asymptotic solution can be presented as the primary inertial mode plus the tangential

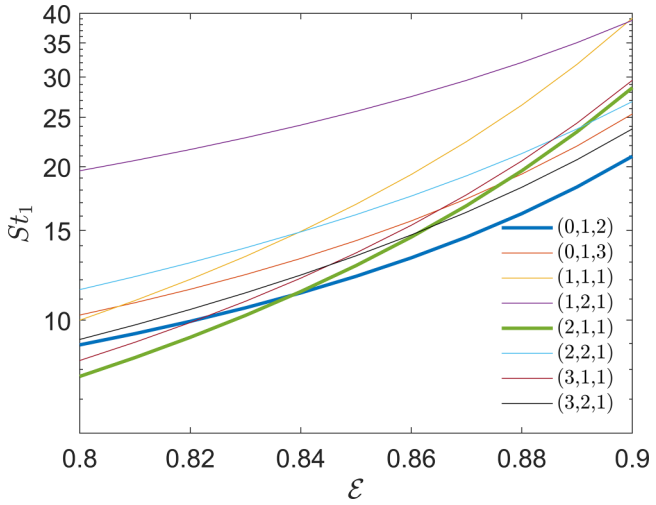

FIG. 1. The critical stratification numbers St_1 of several inertial modes plotted as function of the $\mathcal{E}$ at $\mathrm{Ek} = 10^{-4}$ and $\mathrm{Pr} = 5 \times 10^{-3}$. Modes are distinguished by the set of wave numbers (m, n, k) in the legend. The thick green curve depicts the (2,1,1) wave mode, and the thick blue curve draws the (0,1,2) zonal oscillatory mode. The two thickened curves cross over at about $\mathcal{E} = 0.84$.

components of the boundary layer flow,

$$\boldsymbol{u}_{\mathrm{asym}} = [\boldsymbol{u}_{012} + (\hat{\boldsymbol{\phi}} \cdot \widetilde{\boldsymbol{u}})\hat{\boldsymbol{\phi}} + (\hat{\boldsymbol{\tau}} \cdot \widetilde{\boldsymbol{u}})\hat{\boldsymbol{\tau}}]e^{i2\sigma_{012}t} + \mathrm{c.c.}, \tag{21}$$

in which the inertial mode has the components

$$\sigma_{012} = \sqrt{\frac{3}{7 - 4\mathcal{E}^2}}, \tag{22}$$

$$\begin{aligned}\hat{\boldsymbol{\eta}} \cdot \boldsymbol{u}_{012} = \frac{i\sqrt{\eta^2 + \mathcal{E}^2}}{\sqrt{\eta^2 + \mathcal{E}^2\tau^2}} \Bigg\{ & \frac{15\sigma_{012}}{4\big(1 - \mathcal{E}^2\sigma_{012}^2\big)}(1 - \tau^2)\eta - \frac{105\sigma_{012}\big(1 - \sigma_{012}^2\big)}{16\big(1 - \mathcal{E}^2\sigma_{012}^2\big)^2}(\eta^2 + \mathcal{E}^2)(1 - \tau^2)^2\eta \\ & - \frac{15\sigma_{012}}{2\big(1 - \mathcal{E}^2\sigma_{012}^2\big)}\eta\tau^2 - \frac{105\sigma_{012}}{4\big(1 - \mathcal{E}^2\sigma_{012}^2\big)^2}(1 - \tau^2)\big[\sigma_{012}^2\eta^2 - \big(1 - \sigma_{012}^2\big)(\eta^2 + \mathcal{E}^2)\big]\eta\tau^2 \\ & + \frac{35\sigma_{012}^3}{2\big(1 - \mathcal{E}^2\sigma_{012}^2\big)^2}\eta^3\tau^4\Bigg\},\end{aligned} \tag{23}$$

$$\begin{aligned}\hat{\boldsymbol{\phi}} \cdot \boldsymbol{u}_{012} = \frac{\sqrt{(\eta^2 + \mathcal{E}^2)(1 - \tau^2)}}{1 - \mathcal{E}^2\sigma_{012}^2}\Bigg[& -\frac{15}{4} + \frac{105\big(1 - \sigma_{012}^2\big)}{16\big(1 - \mathcal{E}^2\sigma_{012}^2\big)}(\eta^2 + \mathcal{E}^2)(1 - \tau^2) \\ & + \frac{105\sigma_{012}^2}{4\big(1 - \mathcal{E}^2\sigma_{012}^2\big)}(\eta\tau)^2\Bigg],\end{aligned} \tag{24}$$

$$\begin{aligned}\hat{\boldsymbol{\tau}} \cdot \boldsymbol{u}_{012} = \frac{i\sqrt{1 - \tau^2}}{\sqrt{\eta^2 + \mathcal{E}^2\tau^2}} \Bigg\{ & - \frac{15\sigma_{012}}{4\big(1 - \mathcal{E}^2\sigma_{012}^2\big)}(\eta^2 + \mathcal{E}^2)\tau + \frac{105\sigma_{012}\big(1 - \sigma_{012}^2\big)}{16\big(1 - \mathcal{E}^2\sigma_{012}^2\big)^2}(\eta^2 + \mathcal{E}^2)^2(1 - \tau^2)\tau \\ & - \frac{15\sigma_{012}}{2\big(1 - \mathcal{E}^2\sigma_{012}^2\big)}\eta^2\tau + \frac{105\sigma_{012}}{4\big(1 - \mathcal{E}^2\sigma_{012}^2\big)^2}(\eta^2 + \mathcal{E}^2)\big[\sigma_{012}^2\tau^2 + \big(1 - \sigma_{012}^2\big)(1 - \tau^2)\big]\eta^2\tau \\ & + \frac{35\sigma_{012}^3}{2\big(1 - \mathcal{E}^2\sigma_{012}^2\big)^2}\eta^4\tau^3\Bigg\},\end{aligned} \tag{25}$$

and the tangential components of the boundary layer flow are

$$\hat{\boldsymbol{\tau}}\cdot\tilde{\boldsymbol{u}} = -i\frac{15(7-4\mathcal{E}^2)}{28(1-\mathcal{E}^2)}\left\{\frac{\sqrt{3[1-\mathcal{E}^2(1-\tau^2)]}}{\sqrt{7-4\mathcal{E}^2}}-\tau\right\}\tau\sqrt{1-\tau^2}e^{\gamma_{012}^{+}[(\sqrt{1-\mathcal{E}^2}-\eta)/\sqrt{\mathrm{Ek}}]}$$
$$-i\frac{15(7-4\mathcal{E}^2)}{28(1-\mathcal{E}^2)}\left\{\frac{\sqrt{3[1-\mathcal{E}^2(1-\tau^2)]}}{\sqrt{7-4\mathcal{E}^2}}+\tau\right\}\tau\sqrt{1-\tau^2}e^{\gamma_{012}^{-}[(\sqrt{1-\mathcal{E}^2}-\eta)/\sqrt{\mathrm{Ek}}]}, \tag{26}$$

$$\hat{\boldsymbol{\phi}}\cdot\tilde{\boldsymbol{u}} = +\frac{15(7-4\mathcal{E}^2)}{28(1-\mathcal{E}^2)}\left\{\frac{\sqrt{3[1-\mathcal{E}^2(1-\tau^2)]}}{\sqrt{7-4\mathcal{E}^2}}-\tau\right\}\tau\sqrt{1-\tau^2}e^{\gamma_{012}^{+}[(\sqrt{1-\mathcal{E}^2}-\eta)/\sqrt{\mathrm{Ek}}]}$$
$$-\frac{15(7-4\mathcal{E}^2)}{28(1-\mathcal{E}^2)}\left\{\frac{\sqrt{3[1-\mathcal{E}^2(1-\tau^2)]}}{\sqrt{7-4\mathcal{E}^2}}+\tau\right\}\tau\sqrt{1-\tau^2}e^{\gamma_{012}^{-}[(\sqrt{1-\mathcal{E}^2}-\eta)/\sqrt{\mathrm{Ek}}]}, \tag{27}$$

where the $\gamma_{012}^{\pm}$ coefficients are respectively

$$\gamma_{012}^{+} = -\left(1+i\frac{\sigma_{012}h^2+\tau h}{|\sigma_{012}h^2+\tau h|}\right)\sqrt{|\sigma_{012}h^2+\tau h|}, \tag{28}$$

$$\gamma_{012}^{-} = -\left(1+i\frac{\sigma_{012}h^2-\tau h}{|\sigma_{012}h^2-\tau h|}\right)\sqrt{|\sigma_{012}h^2-\tau h|}, \tag{29}$$

and $h=\sqrt{1-\mathcal{E}^2(1-\tau^2)}$. Note that the boundary layer solution is known to break down at critical latitudes [13]:

$$\tau = \pm\sigma_{012}\frac{\sqrt{1-\mathcal{E}^2}}{\sqrt{1-\sigma_{012}^2\mathcal{E}^2}}. \tag{30}$$

The effects of the breakdown on asymptotic solution were shown to be negligible in spheres [14,15] and spheroids [9].

To confirm the interesting theoretical prediction, numerical calculations are carried out using a three-dimensional finite-element method [16]. The fully nonlinear convection equations,

$$\frac{\partial\boldsymbol{u}_{\mathrm{num}}}{\partial t}+\boldsymbol{u}_{\mathrm{num}}\cdot\nabla\boldsymbol{u}_{\mathrm{num}}+2\hat{\boldsymbol{z}}\times\boldsymbol{u}_{\mathrm{num}}$$
$$=-\nabla p_{\mathrm{num}}+\mathrm{St}[\mathrm{Fr}\hat{\boldsymbol{z}}\times(\hat{\boldsymbol{z}}\times\boldsymbol{r})-\boldsymbol{g}_0]\Theta_{\mathrm{num}}+\mathrm{Ek}\nabla^2\boldsymbol{u}_{\mathrm{num}}, \tag{31}$$

$$\nabla\cdot\boldsymbol{u}_{\mathrm{num}}=0, \tag{32}$$

$$\frac{\partial\Theta_{\mathrm{num}}}{\partial t}+\boldsymbol{u}_{\mathrm{num}}\cdot\nabla(T_0+\Theta_{\mathrm{num}})=\frac{\mathrm{Ek}}{\mathrm{Pr}}\nabla^2\Theta_{\mathrm{num}}, \tag{33}$$

are directly solved in oblate spheroidal geometry $\mathcal{D}=\{(x,y,z)|x^2+y^2+\frac{z^2}{1-\mathcal{E}^2}\leqslant 1\}$. When the parameters Ek, Pr, and Fr and the corresponding tetrahedral finite-element mesh are prescribed, calculations are always initially set to static $\boldsymbol{u}_{\mathrm{num}}(t=0)=\boldsymbol{0}$, but with small random perturbations in temperature. The numerical onset of convection can be obtained by searching for the minimum St at which a finite amplitude of convective motion can be properly excited and sustained. We have tried doing the numerical simulations respectively at $\mathcal{E}=0.8$ (Fr $=0.2724$) and $\mathcal{E}=0.9$ (Fr $=0.3304$). Typical azimuthal flows $\hat{\boldsymbol{\phi}}\cdot\boldsymbol{u}_{\mathrm{num}}$ of the numerical solutions are presented in Fig. 2. The transition from the (2,1,1) mode to the (0,1,2) mode is convincingly demonstrated. Also, the corresponding asymptotic solutions are compared with the numerical solutions in Table I. Finally, nine consecutive snapshots within one full period of the zonal oscillation are demonstrated in Fig. 3, in terms of the azimuthal flow component $\hat{\boldsymbol{\phi}}\cdot\boldsymbol{u}_{\mathrm{num}}$. The meridional wave propagation from the equator towards the polar regions can be seen.

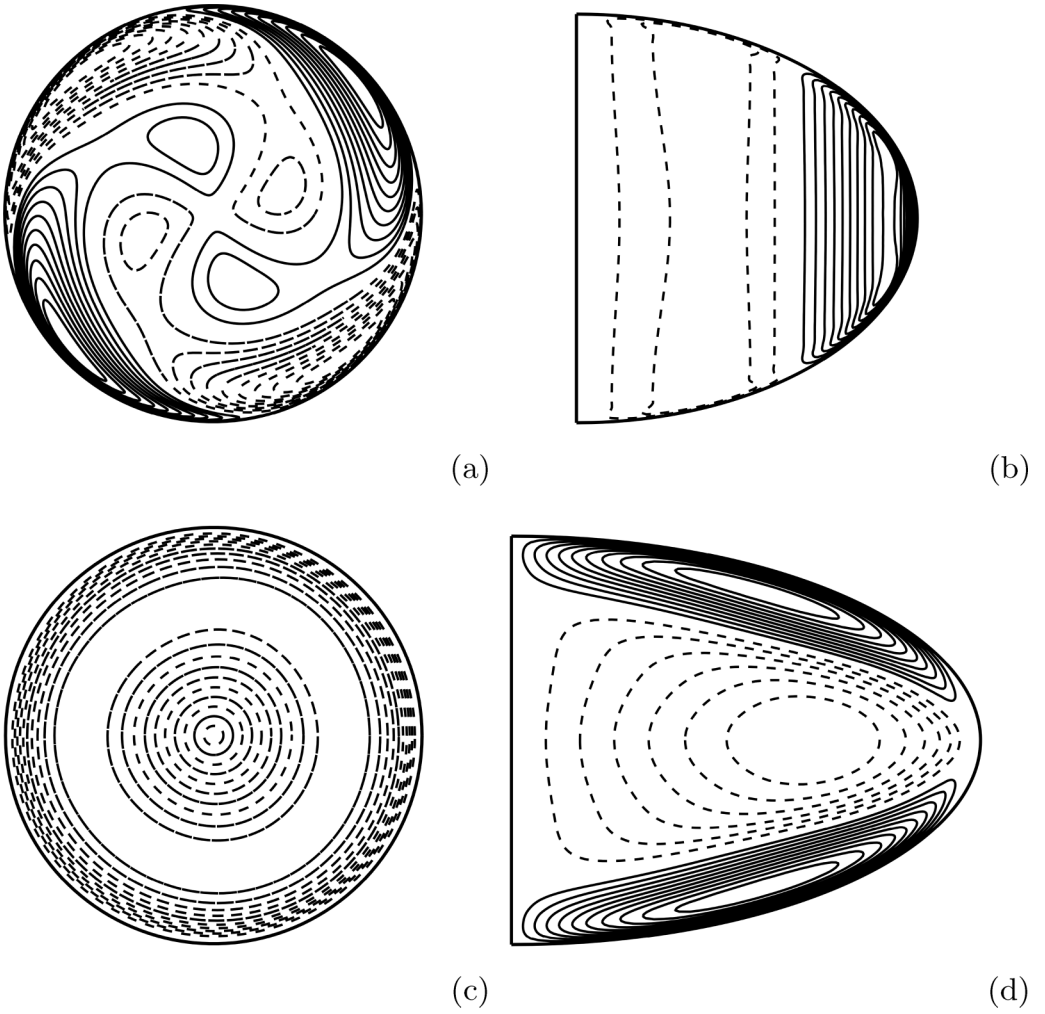

FIG. 2. Contours of the azimuthal component $\hat{\boldsymbol{\phi}} \cdot \boldsymbol{u}_{\rm num}$ are shown in the equatorial plane (the left column) and a meridional cross section (the right column). Solid contours mark positive values, and dashed contours mark negative values. The upper row contains a typical snapshot for the case $\mathcal{E} = 0.8$, while the bottom row plots a typical snapshot for the case $\mathcal{E} = 0.9$.

It is beneficial to consider the physical reason why the pattern of rapidly rotating convection would switch from a non-axisymmetric quasigeostrophic wave to an equatorially symmetric zonal oscillation. For a large Prandtl number, the viscous effect offsets the rotational Taylor-Proudman

TABLE I. Comparison of the global critical parameters of the numerical and asymptotic solutions. The superscript "asym" denotes the result computed with the asymptotic solution, and "num" denotes a numerical result.

Ek	Pr	Fr	$\mathcal{E}$	(m_c, n_c, k_c)	$\mathrm{St}_c^{\rm asym}$	$\mathrm{St}_c^{\rm num}$	$\sigma_c^{\rm asym}$	$\sigma_c^{\rm num}$
		0.2724	0.8	(2,1,1)	7.75	7.85	−0.1152	−0.1017
10^{-4}	5×10^{-3}	0.3304	0.9	(0,1,2)	20.96	20.00	0.8837	0.8840

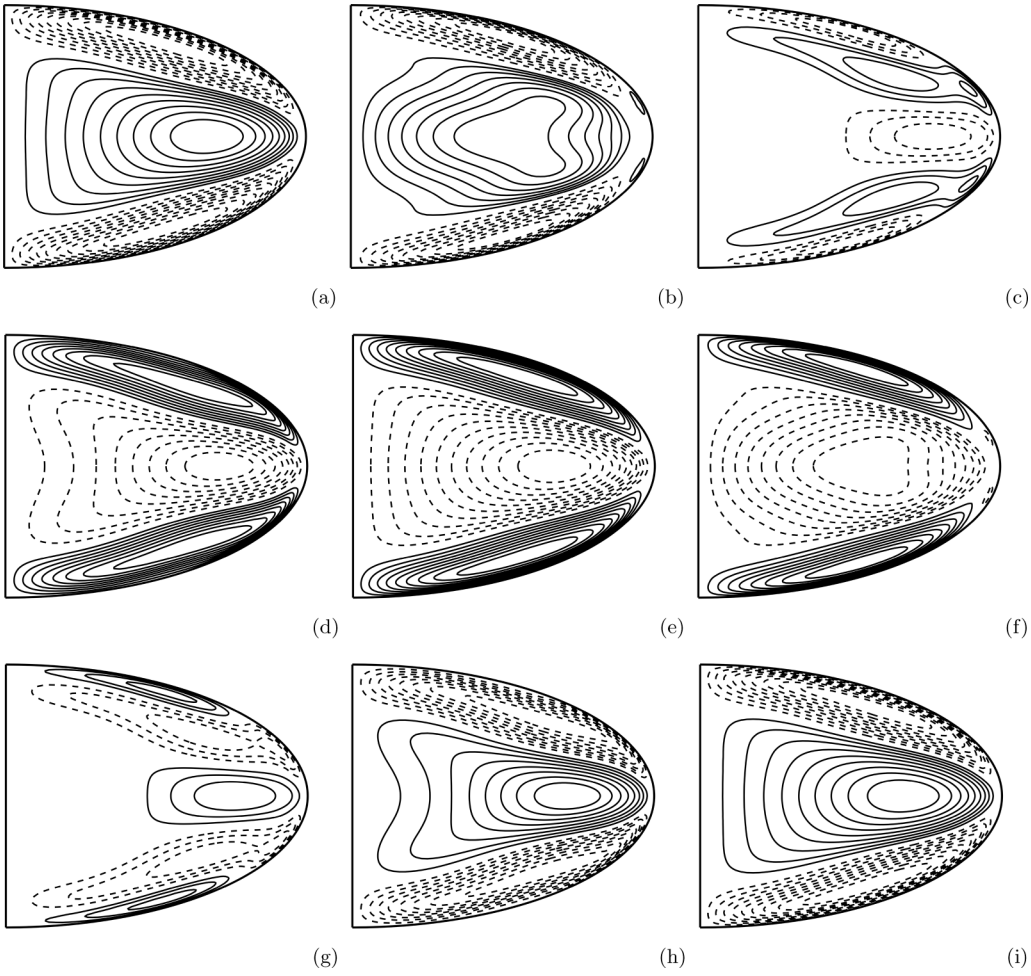

FIG. 3. Panels (a)–(i) plot nine consecutive snapshots of the azimuthal flow $\hat{\boldsymbol{\phi}} \cdot \boldsymbol{u}_{\rm num}$ within one cycle of the zonal oscillation in a meridional cross section of the oblate spheroid of $\mathcal{E} = 0.9$. Solid contours mark positive values, and dashed contours mark negative values.

constraint so that convection can occur. For a moderate or small Prandtl number considered in this Letter, it is mainly the inertial effect that offsets the constraint. Consequently, various patterns become physically realizable.

IV. CONCLUDING REMARKS

For the first time, this research discovers that an equatorially symmetric zonal mode can be physically preferred at the linear onset of thermal instability in a rapidly rotating self-gravitating fluid. This phenomenon is a result of self-consistently considering the nonspherical geometry of the rotating fluid. Therefore, the Froude number is indeed another important parameter for rotating convection in planetary and astrophysical bodies, besides the well-known Ekman number and Prandtl number. However, in the present study, the Ekman and Prandtl numbers are both fixed for illustration. More comprehensive and systematic studies are necessary to understand situations under more combinations of the three parameters. It can be expected that similar axisymmetry at

the onset of rotating convection might exist for lower spheroidal oblateness, which would be more realistic for geophysical and astrophysical objects.

In astrophysics, the convective envelopes of luminous stars are typically marked by a small Prandtl number because radiative heat transfer can effectively cause large thermal diffusivity κ. As a result, stellar convection might belong to the category of inertial convection. This research reveals a new linear mechanism that could directly drive zonal flow and differential rotation in stellar interiors.

ACKNOWLEDGMENTS

This work was supported by the B-type Strategic Priority Program of the Chinese Academy of Sciences (Grant No. XDB41000000), the National Natural Science Foundation of China (Grant No. 12273092), and the Pre-research Project on Civil Aerospace Technologies funded by the China National Space Administration (Grant No. D020303). The computation made use of the high-performance computing resources in the Core Facility for Advanced Research Computing at Shanghai Astronomical Observatory, Chinese Academy of Sciences.

[1] S. Chandrasekhar, *Hydrodynamics and Hydrodynamic Stability* (Clarendon, Oxford, 1961).
[2] P. H. Roberts, On the thermal instability of a rotating-fluid sphere containing heat sources, Philos. Trans. R. Soc. London, A **263**, 93 (1968).
[3] F. Busse, Thermal instabilities in rapidly rotating systems, J. Fluid Mech. **44**, 441 (1970).
[4] F. Garcia, J. Sánchez, and M. Net, Antisymmetric Polar Modes of Thermal Convection in Rotating Spherical Fluid Shells at High Taylor Numbers, Phys. Rev. Lett. **101**, 194501 (2008).
[5] J. Sánchez, F. Garcia, and M. Net, Critical torsional modes of convection in rotating fluid spheres at high Taylor numbers, J. Fluid Mech. **791**, R1 (2016).
[6] W. Zhu, C. X. Huang, G. Zhou, and D. N. C. Lin, Constraining the oblateness of *Kepler* planets, Astrophys. J. **796**, 67 (2014).
[7] P. Kervella, A. Domiciano de Souza, S. Kanaan *et al.*, The environment of the fast rotating star Achernar. II. Thermal infrared interferometry with VLTI/MIDI, Astron. Astrophys. **493**, L53 (2009).
[8] D. Kong, Rapidly rotating self-gravitating Boussinesq fluid: A nonspherical model of motionless stable stratification, Phys. Rev. Fluids **7**, 074803 (2022).
[9] W. Li and D. Kong, Rapidly rotating self-gravitating Boussinesq fluid. II. Onset of thermal inertial convection in oblate spheroidal cavities, Phys. Rev. Fluids **7**, 103502 (2022).
[10] H. Lamb, *Hydrodynamics*, Dover Books on Physics (Dover, New York, 1945).
[11] K. Zhang, X. Liao, and P. Earnshaw, On inertial waves and oscillations in a rapidly rotating spheroid, J. Fluid Mech. **504**, 1 (1999).
[12] C. Flammer, *Spheroidal Wave Functions* (Stanford University, Stanford, CA, 1957).
[13] P. H. Roberts, On the thermal instability of a highly rotating fluid sphere, Astrophys. J. **141**, 240 (1965).
[14] K. Zhang, On coupling between the Poincaré equation and the heat equation: non-slip boundary condition, J. Fluid Mech. **284**, 239 (1995).
[15] K. Zhang, X. Liao, and F. H. Busse, Asymptotic solutions of convection in rapidly rotating non-slip spheres, J. Fluid Mech. **578**, 371 (2007).
[16] K. H. Chan, K. Zhang, and X. Liao, An EBE finite element method for simulating nonlinear flows in rotating spheroidal cavities, Int. J. Numer. Methods Fluids **63**, 395 (2010).